Available online at www.sciencedirect.com
SCIENCE DIRECT
Sensors and Actuators A 125 (2006) 178–185
SENSORS AND ACTUATORS A PHYSICAL
www.elsevier.com/locate/sna

Effects of corner frequency on bandwidth and resonance amplitude in designing PZT thin-film actuators

Chia-Che Wu [a], Cheng-Chun Lee [a], G.Z. Cao [b], I.Y. Shen [a,*]

[a] *Department of Mechanical Engineering, University of Washington, Box 362600, Seattle, WA 98195-2600, USA*
[b] *Department of Material Science and Engineering, University of Washington, Seattle, WA 98195-2120, USA*

Received 26 February 2005; received in revised form 5 July 2005; accepted 5 July 2005
Available online 26 August 2005

Abstract

In the last decade, lead zirconate titanate oxide (PZT) thin-film actuators have received increasing attention because of their high frequency bandwidth, large actuation strength, fast response, and small size. The PZT film thickness is usually less than several microns as opposed to hundreds of microns for bulk PZT patches that are commercially available. As a result, PZT thin-film actuators pose unique vibration issues that do not appear in actuators with bulk PZT. Two major issues affecting actuator performance are the frequency bandwidth and the resonance amplitude. As an electromechanical device, a PZT thin-film actuator's bandwidth and resonance amplitude depend not only on the lowest natural frequency ω_n of the actuator's mechanical structure but also on the corner frequency ω_c of the actuator's *RC*-circuit. For PZT thin-film actuators, the small film thickness implies large film capacitance C and small ω_c. When the size of the actuator decreases, ω_n increases dramatically. As a result, improper design of PZT thin-film actuators could lead to $\omega_c \ll \omega_n$ substantially reducing the actuator bandwidth and the resonance amplitude. This paper is to demonstrate this phenomenon through theoretical analyses and calibrated experiments. In the theoretical analyses, frequency response functions of a PZT thin-film actuator are obtained to predict 3 dB actuator bandwidth and resonance amplitude for cases when $\omega_c \ll \omega_n$, $\omega_c \approx \omega_n$ and $\omega_c \gg \omega_n$. In the experiments, frequency response functions of a fixed–fixed silicon beam with a 1 μm thick PZT film are measured through use of a laser Doppler vibrometer and a spectrum analyzer. The silicon beam has multiple electrodes with a wide range of resistance R and corner frequency ω_c. The experimental results confirm that the actuator bandwidth and resonance amplitude are substantially reduced when $\omega_c \ll \omega_n$.

Keywords: Corner frequency; Bandwidth; Resonance amplitude; PZT thin-film; Actuators; *RC* circuit; Frequency response functions

1. Introduction

Lead zirconate titanate oxide ($PbZr_{1-x}Ti_xO_3$ or PZT) thin-film actuators have received increasing attention in the last decade because of their wide applications, such as atomic force microscopes (AFM) [1,2], ultrasonic micromotors [3–6], one- or two-dimensional scanners [7–9], microswitches [10], resonators [11,12], and dual-stage actuators/sliders for next-generation computer hard disk drives [13–15]. Compared with traditional MEMS-based microactuators, PZT thin-film actuators have higher frequency bandwidth, larger actuation strength, and faster response. According to [16], there are four types of microactuators: thermal, shape-memory-alloy (SMA), electrostatic, and piezoelectric (specifically PZT). Thermal and SMA actuators have low frequency bandwidth [16] (<1 kHz), whereas electrostatic and PZT actuators have high frequency bandwidth (>1 kHz). Moreover, electrostatic actuators have much smaller actuation force and energy density than PZT films (3.4×10^3 J/m^3 for electrostatic actuators versus 1.2×10^5 J/m^3 for PZT [16]).

Functionally, PZT thin-film actuators can be classified as broadband actuators and single-frequency actuators. Fig. 1 shows a frequency response function (FRF) explaining the differences of these two types of actuators. Broadband actuators operate over a wide range of frequency, in which the frequency response function is approximately constant.

* Corresponding author. Tel.: +1 206 543 5718; fax: +1 206 685 8047.
E-mail address: ishen@u.washington.edu (I.Y. Shen).

0924-4247/$ – see front matter © 2005 Elsevier B.V. All rights reserved.
doi:10.1016/j.sna.2005.07.007

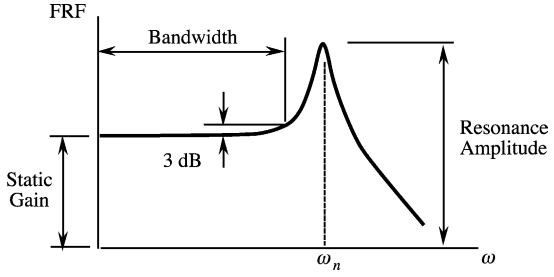

Fig. 1. Frequency range of broadband and single-frequency actuators.

In this frequency range, the actuator output motion is proportional to the input voltage without significant distortion. The bandwidth of the actuator is often defined as the frequency range in which the FRF has less than 3-dB variation to minimize possible input–output distortion. Applications of broadband actuators include AFM and microswitches for example. In this case, maximizing the bandwidth is a major design consideration because it determines how fast the tip of AFM can tap and how fast a microswitch can open and close. In contrast, single-frequency actuators operate at a single frequency, usually at a natural frequency of the actuator's mechanical structure. Example applications include resonators and scanners. In these applications, the resonance amplitude is very critical. Large resonance amplitude, for example, implies that a scanner can have a large scanning angle.

Since PZT thin-film actuators are electromechanical devices, the actuators' performance indexes, such as bandwidth and resonance amplitude, depend not only on the actuators' mechanical structures but also on actuators' circuit design. Mechanically, the structure is a spring–mass–damper system characterized by the lowest natural frequency ω_n. Electrically, the circuit forms a low-pass *RC* filter characterized by its corner frequency ω_c. For actuators employing bulk PZT, ω_c is often a couple of orders higher than ω_n. Therefore, the actuator bandwidth and resonance amplitude are primarily dominated by the mechanical resonance frequency ω_n and the system's damping, respectively.

For PZT thin-film actuators, however, ω_c could be a couple of orders-of-magnitude less than ω_n due to the tiny thickness of PZT films. Traditional bulk PZT often appears as thin patches with thickness no less than 80 μm. In contrast, thickness of PZT thin films can vary quite substantially depending on their fabrication methods. PZT films derived from sol–gel processes – a common fabrication method for PZT films – usually have thickness less than 1 μm. As a result, the capacitance *C* of PZT thin films is significantly larger than that of bulk PZT on a per area basis, and the corner frequency ω_c of PZT thin-film actuators is reduced dramatically. As the size of PZT thin-film actuators decreases, ω_n increases significantly. Therefore, improper design of PZT thin-film actuators could lead to $\omega_c \ll \omega_n$ substantially reducing the actuator bandwidth and resonance amplitude. These negative effects of the corner frequency ω_c on bandwidth and resonance amplitude, however, have not been properly addressed in the literature of PZT thin-film actuators thus far [1–15].

The purpose of this paper is to demonstrate the negative effects of the corner frequency ω_c on bandwidth and resonance amplitude through theoretical analysis and calibrated experiments. For the rest of the paper, we will first explain two competing frequencies ω_c and ω_n. A Matlab simulation shows how relative magnitude of ω_c and ω_n would affect the overall frequency response function, the actuator bandwidth, and the resonance amplitude. Then we demonstrate the negative effects of low ω_c by conducting an experiment on a matrix of fixed–fixed silicon beams with PZT thin films that offer a wide range of ω_c and ω_n. A laser Doppler vibrometer and a spectrum analyzer measure frequency response functions to determine the actuator bandwidth.

2. Theoretical analysis

Exact modeling of piezoelectric actuators is in fact a very difficult task. In traditional filter applications, piezoelectric actuators serve as resonators vibrating in resonance. When a piezoelectric actuator is close to its resonance, significant electromechanical coupling appears. As a result, electrical response of the piezoelectric actuator can be modeled through an equivalent *RLC* circuit in parallel with the capacitance of the piezoelectric actuator, where the equivalent *RLC* circuit approximates the inertia, stiffness, and damping effects of the piezoelectric actuator near the resonance [17,18]. This approach, however, does not apply to the current analysis of bandwidth when $\omega_c \ll \omega_n$, because the resonance condition is not maintained. When the piezoelectric actuator is off resonance, the electromechanical coupling can be simply approximated as a sequence of two block diagrams as shown in Fig. 2. The block diagrams consist of an electrical model cascaded with a mechanical model. They are explained in detailed as follows.

For the electrical model, it is a simple *RC*-circuit. The circuit of the PZT thin-film actuator consists of a resistor and a capacitor in serial combination. The resistor with resistance *R* simulates the resistance of the actuator circuit, and the capacitor with capacitance *C* models the dielectric property of the PZT film. In addition, an input voltage $v_i(t)$ drives the PZT thin-film actuator circuit. Because of the presence of the resistance *R* and capacitance *C*, the actual voltage $v_c(t)$ physically driving the PZT film will not be equal to the input voltage $v_i(t)$. When the driving voltage is sinusoidal, i.e., $v_i(t) = V_i(\omega)e^{j\omega t}$ and $v_c(t) = V_c(\omega)e^{j\omega t}$, the output and input voltages are related through the electric frequency response function $H_e(\omega)$

$$H_e(\omega) = \frac{V_c(\omega)}{V_i(\omega)} = \frac{1}{1 + j\omega RC} \tag{1}$$

with magnitude

$$|H_e(\omega)| = \frac{1}{\sqrt{1 + (\omega/\omega_c)^2}} \tag{2}$$

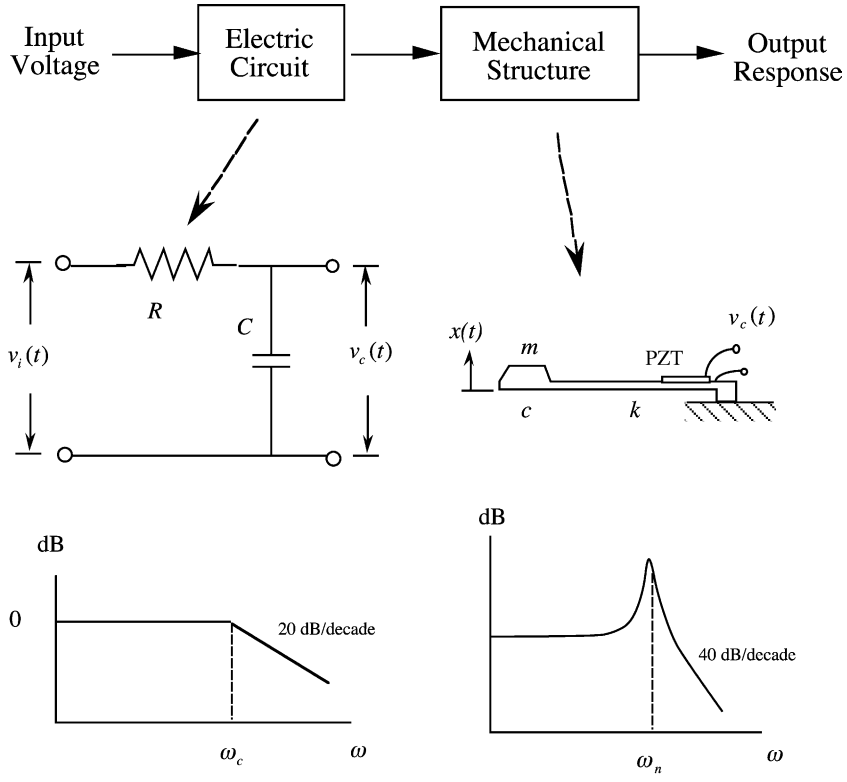

Fig. 2. Block diagrams of PZT thin-film actuators.

where $\omega_c \equiv 1/RC$ is the corner frequency (also known as the cut-off frequency in filter or circuit design).

There are several issues worth noting for the electrical model. First, the *RC*-circuit forms a low-pass filter whose frequency response function is shown in Fig. 2. In other words, $V_c(\omega) \approx V_i(\omega)$ for $\omega \ll \omega_c$ and ω_c is the 3 dB point defining the bandwidth of the *RC*-circuit. Second, the small thickness of PZT film substantially reduces the corner frequency ω_c. Since PZT thin film is dielectric, the capacitance C can be estimated through $C = \varepsilon A/d$, where ε, d, and A are the dielectric constant, thickness, and area of the PZT film, respectively. Now let us consider two PZT films with the same film area A and same dielectric constant ε but different thickness d. The one with smaller film thickness will have larger capacitance. If the two PZT thin films have the same external circuit, the PZT film with smaller thickness will have a smaller corner frequency and hence a smaller electrical bandwidth. Third, the electrical circuit of PZT thin-film actuators tends to have larger resistance R than that of actuators with bulk PZT. The major resistance of the circuit results from thin conductive wires. For PZT thin-film actuators, these conductive wires appear in the form of printed metal layers with thickness less than 1 μm. For bulk PZT actuators, their lead wires are at least one-order-of-magnitude larger in every dimension than those of PZT thin-film actuators. As a result, the thin conductive wires with PZT thin-film actuators have much higher resistance because $R = l/A\sigma$, where l, A, and σ are the length, the cross-sectional area, and the conductivity of the conductive wires, respectively. Since the resistance R is higher, PZT thin-film actuators have smaller corner frequency and the electrical frequency bandwidth.

For the mechanical model, the PZT thin-film actuator is often modeled as a vibrating mechanical structure driven by a PZT film with input voltage $v_c(t)$. The input voltage $v_c(t)$ deforms the PZT film mechanically. The deformation of the PZT film then drives the mechanical structure resulting in deflection $x(t)$ There are several issues worth noting.

First, the mechanical structure, in many occasions, can be modeled as a simple one-degree-of freedom system shown in Fig. 2. When the system is under sinusoidal excitations, i.e., $v_c(t) = V_c(\omega)e^{j\omega t}$ and $x(t) = X(\omega)e^{j\omega t}$, the resulting mechanical frequency response function will take the form

$$H_m(\omega) = \frac{X(\omega)}{V_c(\omega)} = \frac{X_0}{1 - \left(\frac{\omega}{\omega_n}\right)^2 + j\left(\frac{2\varsigma\omega}{\omega_n}\right)} \tag{3}$$

where X_0 is the static gain of $H_m(\omega)$ and ς is the viscous damping factor. Moreover, ω_n dominates the mechanical bandwidth of the actuator, as revealed from $|H_m(\omega)|$ shown in Fig. 2. Furthermore, the resonance amplitude is

$$|H_m(\omega_n)| = \frac{X_0}{2\varsigma} \tag{4}$$

Although realistic mechanical structures have many natural frequencies, the lowest natural frequency ω_n is often the most critical frequency in defining the mechanical band-

width.Second, natural frequency ω_n increases dramatically when the size of the mechanical structure decreases. Theoretically, ω_n^2 is the ratio between the restoring force and the inertia force when a mechanical system undergoes free sinusoidal oscillations. If the mechanical structure is reduced in size, the inertia force diminishes much faster than the restoring force. As a result, microactuators usually have significantly higher ω_n than bulk actuators. For example, let us consider a cantilever beam with a rectangular cross section. The cantilever has length l, width b, height h, Young's modulus E, and mass density ρ. The lowest natural frequency is

$$\omega_n = \frac{1.875^2}{\sqrt{12}}\sqrt{\frac{E}{\rho}}\frac{h}{l^2} \quad (5)$$

When the cantilever reduces its size in all dimensions, l^2 decreases faster than h. As a result, the natural frequency increases as the size of the cantilever decreases.

According to the block diagram in Fig. 2, the bandwidth and resonance amplitude of a piezoelectric actuator is indeed determined by the minimum of ω_n and ω_c. For actuators with bulk PZT, it is often that $\omega_c \gg \omega_n$. In this case, the design of actuator's mechanical structure is more critical than that of the electrical circuit. For PZT thin-film actuators, ω_c can be in the same order-of-magnitude or even substantially less than ω_n. In this case, the electric circuit needs to be redesigned in order not to sacrifice the actuator bandwidth and the resonance amplitude.

To demonstrate this phenomenon, Fig. 3 compares the magnitude of the composite frequency response function $H_e(\omega)H_m(\omega)$ for $\omega_c \ll \omega_n$ and $\omega_c \gg \omega_n$. The thick solid line is frequency response for $\omega_c = 398$ kHz and $\omega_n = 40$ kHz (i.e., $\omega_c \gg \omega_n$). In this case, the 3 dB bandwidth is 21.5 kHz and the bandwidth is primarily controlled by ω_n. Also, the resonance amplitude is 2×10^{-10} m/V. The thin solid line is frequency response for $\omega_c = 8.29$ kHz and $\omega_n = 40$ kHz (i.e., $\omega_c \ll \omega_n$). In this case, the magnitude starts to decrease at a much lower frequency, and the 3 dB bandwidth is 9 kHz. The bandwidth is primarily controlled by ω_c. Moreover, the resonance amplitude is reduced to 3×10^{-11} m/V—almost an order-of-magnitude reduction.

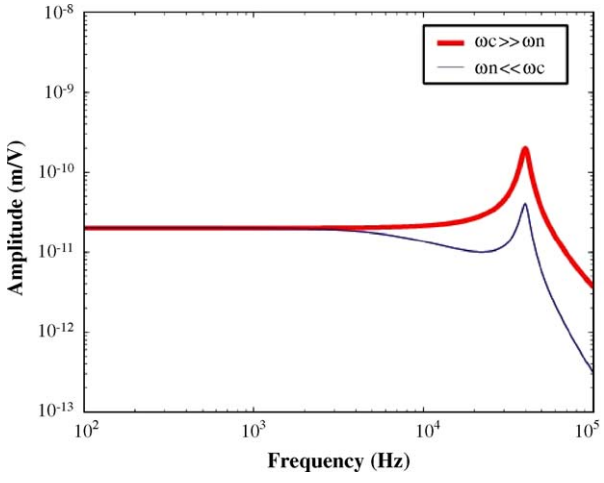

Fig. 3. Composite frequency response function $H_e(\omega)H_m(\omega)$ for $\omega_c \ll \omega_n$ and $\omega_c \gg \omega_n$.

3. Experimental demonstration

Fabrication of the specimen follows an improved sol–gel process [19] shown in Fig. 4. The silicon substrate is first oxidized in a furnace at 1045 °C for 2 h to grow a SiO_2 layer of 500 nm thick. Then a silicon nitride layer of 200 nm thick is deposited by PECVD (plasma enhanced chemical vapor deposition). The bottom electrode consists of Pt/Ti layers with thickness of 100 and 50 nm, respectively. The PZT film is dip-coated three times. For the first two coatings, the sintering temperature is 650 °C for 15 min. For the third coating, the sol is diluted 50% by acetic acid and sintering temperature is 450 °C for 10 min. The philosophy is to use the rapid thermal annealing for the first two coatings to reduce thermal stresses. For the third coating, we used diluted sol to seal possible cracks formed in the previous coatings. Finally, the top electrode consists of Au/Cr layers through evaporation. The thickness of the Au and Cr layers is 50 and 20 nm, respectively. As shown in Fig. 5 the top electrode consists of a square effective electrode, a long connecting electrode, and a rectangular soldering area. The effective electrode is the area where major actuation takes place, and it has dimensions of 4 mm × 4 mm. The connecting electrode has length

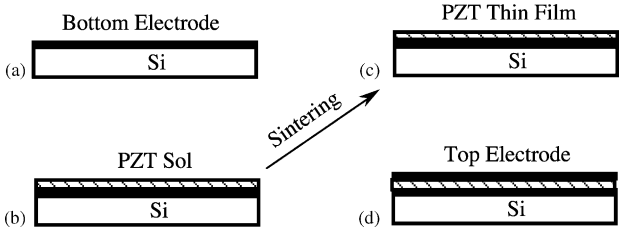

Fig. 4. Sol–gel processes to make PZT thin films.

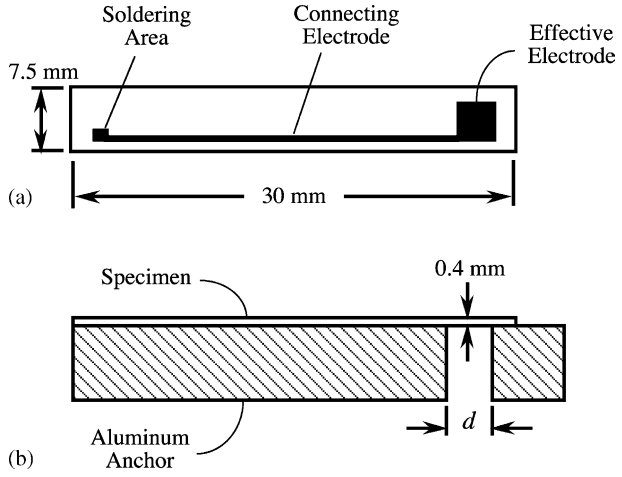

Fig. 5. Specimen used in the experiments: (a) top view and (b) side view.

Table 1
Test matrix in the experiments

Span	Resistance	
	Low (0.3 Ω)	High (480 Ω)
d = 6 mm	ω_c = 1.326 MHz ω_n = 50.92 kHz	ω_c = 8.289 kHz ω_n = 50.92 kHz
d = 15 mm	ω_c = 1.326 MHz ω_n = 12.32 kHz	ω_c = 8.289 kHz ω_n = 12.32 kHz

of 32.91 mm and width of 50 μm. The soldering area has dimensions of 0.5 mm × 1 mm. The measured capacitance of the electrode is 40 nF. The measured resistance between the effective electrode and the soldering pad is 480 Ω.

After the PZT thin film is fabricated, the silicon wafer is diced into rectangular specimen with dimensions 30 mm × 7.5 mm × 0.4 mm. The specimen is anchored at both ends via double stick tapes to simulate fixed–fixed boundary conditions. The span (i.e., distance between the anchors) d can vary from one specimen to another to adjust the lowest natural frequency ω_n of the specimen. Table 1 shows the test matrix. There are two parameters in the text matrix: span d and the electrode resistance R.

For span d, the test set up adopts two different spans: 6 and 15 mm. Based on these configurations, a finite element model is created to predict the lowest natural frequency ω_n and the corresponding mode shape, so that the spot with the largest vibration amplitude can be identified. Note that the span of the specimens is in the same order-of-magnitude with the specimens' width (e.g., 6 mm vs. 7.5 mm). With such aspect ratios, the specimens vibrate more like a plate. Exact solutions based on Euler–Bernoulli beam theory with fixed–fixed boundary conditions can deviate substantially from the experimental results. Therefore, a finite element analysis is preferred over the exact solutions.

The finite element model consists of two portions: the silicon substrate and the anchor. The silicon substrate has thickness of 406 μm. The anchor in the form of double stick tape has a thickness of 100 μm. Table 2 lists the Young's modulus, density, and Poisson's ratio of the silicon substrate and the anchor assumed in the finite element analysis. The PZT thin film is neglected in the finite element model because of its small thickness.

A convergence test is also conducted on the finite element model. The area of the beam span is model by a set of $N \times N$ meshes, where N is the number of element across the beam span and also across the beam width. Fig. 6 shows how the lowest natural frequency varies with respect to the number of elements used in the beam span area, when the span is 6 and 15 mm, respectively. As the number of the element increases to 64, the natural frequency very much converges to a constant.

Table 2
Material properties used in the finite element analysis

	Thickness (μm)	Material properties
Silicon substrate	406	Young's modulus = 110 GPa; Poisson ratio = 0.278; Density = 2330 kg/m^3
Anchor via double stick tape	100	Young's modulus = 3 GPa; Poisson ratio = 0.28; Density = 1000 kg/m^3

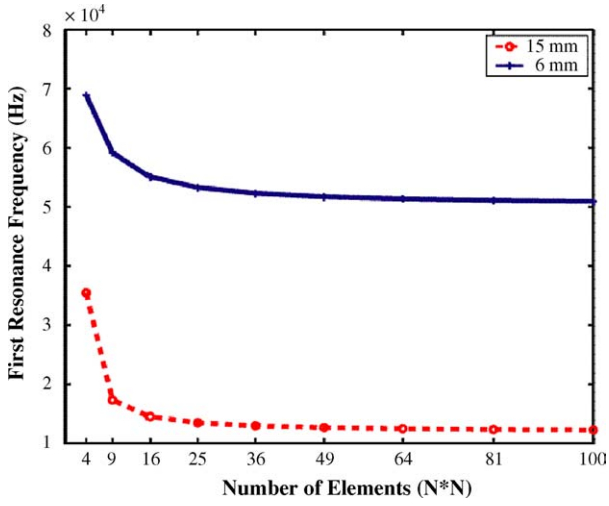

Fig. 6. Convergence test of the finite element model.

The finite element analysis shows that the specimen with the 6 mm span results in ω_n = 50.92 kHz. Fig. 7 shows the corresponding mode shape. Note that the flat regions in Fig. 7 are areas attached to the aluminum anchors. The finite element result indicates that the largest vibration occurs at the free edge of the specimen roughly at the mid-span. This result confirms that the specimen vibrates more like a plate than a fixed–fixed beam. The specimen with the 15 mm span results in ω_n = 12.32 kHz. Fig. 8 shows the corresponding mode shape. Again, the flat regions are attached to the aluminum anchors. The mode shape indicates that the largest vibration occurs uniformly at the mid-span of the specimen.

For electrode resistance R, the test setup adopts two different resistance levels: high resistance 480 Ω and low resistance 0.3 Ω. For the high resistance, the lead wire is soldered to the soldering pad in Fig. 5. The resulting corner frequency is ω_c = 8.289 kHz. For the low resistance, the lead wire is soldered directly onto the effective electrode shown in Fig. 5. The resulting corner frequency is ω_c = 1.326 MHz. Note that the case with high resistance and short span will lead to $\omega_c \ll \omega_n$.

Fig. 9 shows the experimental set up to measure the frequency response functions of the specimen. A spectrum analyzer generates a swept-sine signal to drive the PZT film through an amplifier. The swept-sine sweeps from 1 to 100 kHz. In the meantime, a laser Doppler vibrometer measures the vibration of the specimen at the point of largest vibration. Both the swept-sine signal and the vibrometer measurement are fed back to the spectrum analyzer to calculate the frequency response function.

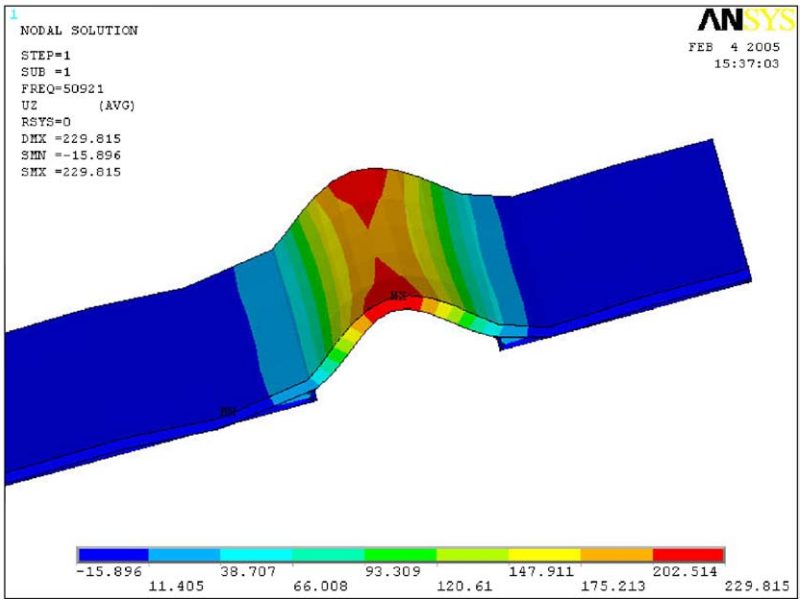

Fig. 7. Lowest mode shape when $d = 6$ mm.

Fig. 10 compares the frequency response functions (FRF) when the span d is 15 mm. In Fig. 10, the thick solid line represents the FRF from the low resistance. According to Table 1, $\omega_c \gg \omega_n$; therefore, the FRF starts with a constant magnitude and is followed by a resonance peak at ω_n. The 3 dB bandwidth is roughly 6.88 kHz. In contrast, the thin solid line in Fig. 10 represents the FRF corresponding to the specimen with high resistance. For the high-resistance case, ω_c is slightly smaller than ω_n. As a result, the FRF starts with a constant magnitude at low frequency, but the magnitude gradually decreases as the driving frequency increases. The 3 dB bandwidth remains roughly the same even the corner frequency ω_c is reduced. The resonance amplitude, however, shows appreciable reduction.

Fig. 11 compares the FRF when the span d is 6 mm. In Fig. 11, the thick solid line represents the FRF from the low resistance. According to Table 1, $\omega_c \gg \omega_n$; therefore, the FRF starts with a constant magnitude and is followed by a resonance peak at ω_n. The 3 dB bandwidth is roughly 23.716 kHz. In contrast, the thin solid line in Fig. 11 represents the FRF corresponding to the specimen with high resistance. According to Table 1, $\omega_c \ll \omega_n$. As a result, the FRF starts with a constant magnitude at low frequency, but the magnitude rapidly decreases as the driving frequency increases. The 3 dB

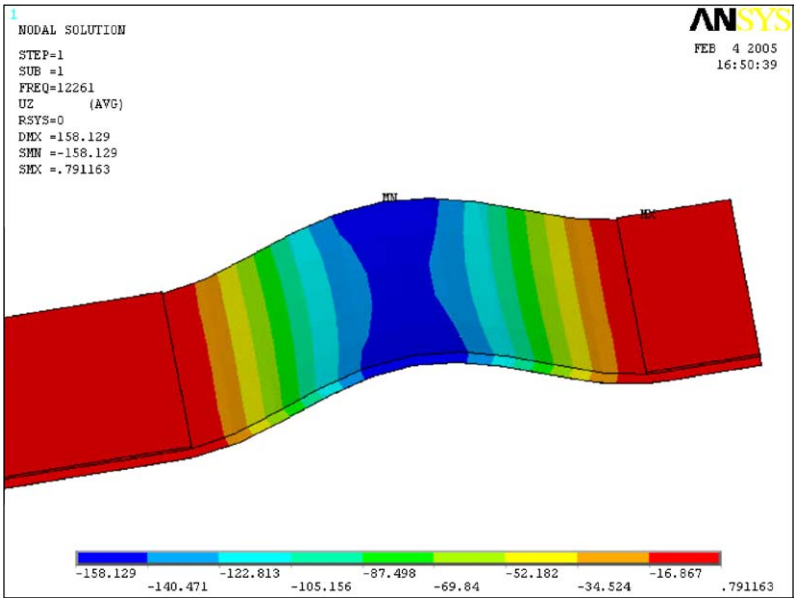

Fig. 8. Lowest mode shape when $d = 15$ mm.

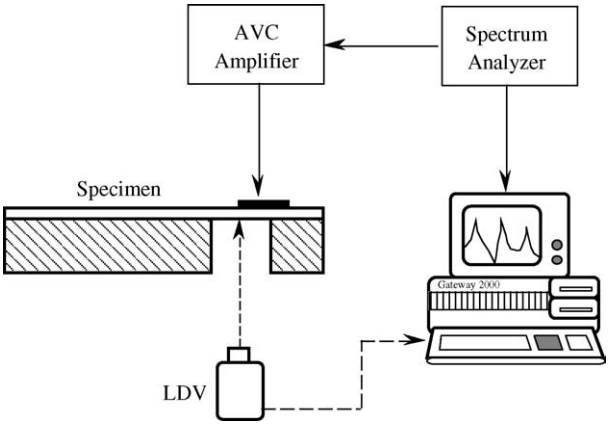

Fig. 9. Experimental set up.

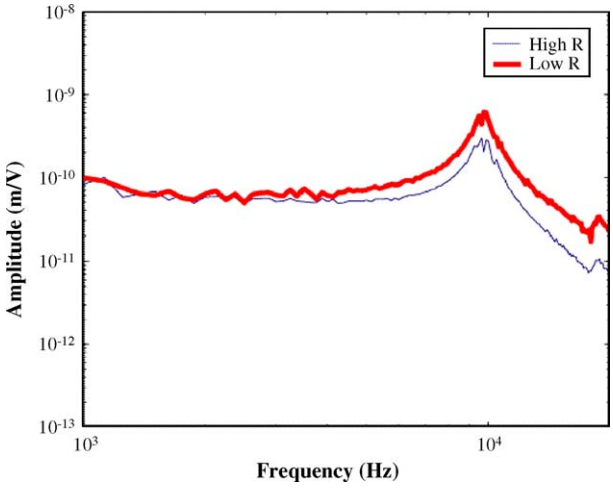

Fig. 10. Frequency response functions for specimen with span $d = 5$ mm.

bandwidth is roughly 9.548 kHz. In other words, the bandwidth has reduced by 59.74% as a result of the high electrical resistance. Moreover, the resonance amplitude has a reduction of one order of magnitude. Figs. 10 and 11 show that the minimum of ω_c and ω_n govern the bandwidth and resonance amplitude of the PZT thin-film actuators.

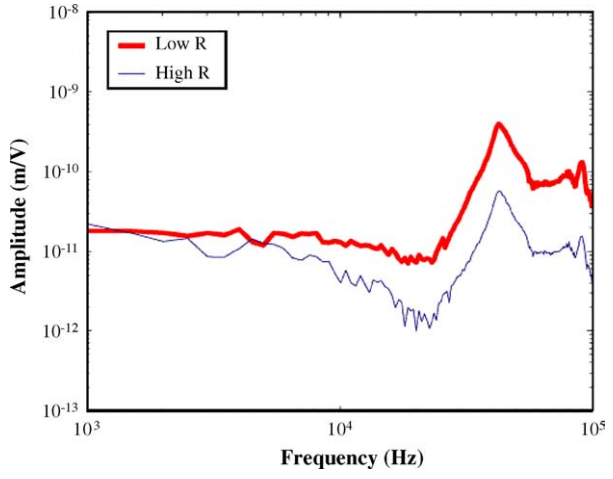

Fig. 11. Frequency response functions for specimen with span $d = 6$ mm.

4. Conclusions

Frequency response of PZT thin-film actuators primarily depends on two frequency parameters ω_n and ω_c, where ω_n is the lowest natural frequency of the actuator's mechanical structure and ω_c is the corner frequency of the electric *RC*-circuit of the actuator. The bandwidth of PZT thin-film actuators is limited by the smaller value of ω_n and ω_c. The resonance amplitude will be reduced when ω_c is less than ω_n. The amount of reduction depends on the difference in ω_c and ω_n.

References

[1] H. Kueppers, T. Leuerer, U. Schnakenberg, W. Mokwa, M. Hoffmann, T. Schneller, U. Boettger, R. Waser, PZT thin films for piezoelectric microactuator applications, Sens. Actuators A 97/98 (2002) 684–690.
[2] T. Shibata, K. Unno, E. Makino, S. Shimada, Fabrication and characterization of diamond AFM probe integrated with PZT thin film sensor and actuator, Sens. Actuators A 114 (2004) 398–405.
[3] A.M. Flynn, L.S. Tavrow, S.F. Bart, R.A. Brooks, D.J. Ehrlich, K.R. Udayakumar, L.E. Cross, Piezoelectric micromotors for microrobots, J. Microelectromech. Syst. 1 (1992) 44–51.
[4] P. Muralt, M. Kohli, T. Maeder, A. Kholkin, K. Brooks, N. Setter, R. Luthier, Fabrication and characterization of PZT thin-film vibrators for micromotors, Sens. Actuators A 48 (1995) 157–165.
[5] P. Muralt, A. Kholkin, M. Kohli, T. Maeder, Piezoelectric actuation of PZT thin-film diaphragms at static and resonant conditions, Sens. Actuators A 53 (1996) 398–404.
[6] M. Dubois, P. Muralt, PZT thin film actuated elastic fin micromotor, IEEE Trans. Ultrason. Ferroelect. Frequency Contr. 45 (1998) 1169–1177.
[7] H. Goto, Two-dimensional micro-optical scanner excited by PZT thin film microactuator, in: Proceedings of SPIE Conference on Optoelectronic Materials and Devices, vol. 3419, 1998, pp. 227–235.
[8] A. Schroth, C. Lee, S. Matsumoto, R. Maeda, Application of sol–gel deposited thin PZT film for actuation of ID and 2D scanners, Sens. Actuators A 73 (1999) 1440152.
[9] J. Tsaur, L. Zhang, R. Maeda, S. Matsumoto, S. Khumpuang, Design and fabrication of ID and 2D micro-scanners actuated by double layered lead zirconate titanate (PZT) bimorph beams, Jpn. J. Appl. Phys. 41 (2002) 4321–4326.
[10] S.J. Gross, S. Tadigadapa, T.N. Jackson, S. Trolier-McKinstry, Q.Q. Zhang, Lead–zirconate–titanate-based piezoelectric micromachined switch, Appl. Phys. Lett. 83 (2003) 174–176.
[11] Q.Q. Zhang, S.J. Gross, S. Tadigadapa, T.N. Jackson, F.T. Djuth, S. Trolier-McKinstry, Lead zirconate titanate films for d_{33} mode cantilever actuators, Sens. Actuators A 105 (2003) 91–97.
[12] F.F.C. Duval, R.A. Dorey, R.W. Wright, Z. Huang, R.W. Whatmore, Fabrication and modeling of high-frequency PZT composite thick film membrane resonators, IEEE Trans. Ultrason. Ferroelect. Frequency Contr. 51 (2004) 1255–1261.
[13] H. Kuwajima, K. Matsuoka, Thin-film piezoelectric DSA for HDD, IEEE Trans. Magn. 38 (2002) 2186–2188.
[14] N. Tagawa, K. Kitamura, A. Mori, Design and fabrication of MEMS-based active slider using double-layered composite PZT thin film in hard disk drives, IEEE Trans. Magn. 39 (2003) 926–931.

[15] K. Suzuki, R. Maeda, J. Chu, T. Kato, M. Kurita, An active head slider using a piezoelectric cantilever for in situ flying-height control, IEEE Trans. Magn. 39 (2003) 826–831.
[16] P. Krulevitch, A.P. Lee, P.B. Ramsey, J.C. Trevino, J. Hamilton, M.A. Northrup, Thin film shape memory alloy microactuators, J. Microelectromech. 5 (1996) 270–282.
[17] T.L. Jordan, Z. Ounaies, Piezoelectric Ceramics Characterization, NASA/CR-2001-211225 ICASE Report, No. 2001-28.
[18] R.C. Buchanan, Ceramic Materials for Electronics, Marcel Dekker, 1986, pp. 189–190.
[19] Y.C. Hsu, C.C. Wu, C.C. Lee, G.Z. Cao, I.Y. Shen, Demonstration and characterization of PZT thin-film sensors and actuators for meso- and micro-structures, Sens. Actuators A: Phys. 116 (3) (2004) 367–377.

Biographies

Chia-Che Wu (Joseph) received an MSME degree from National Chung-Hsien University, Taiwan, in 1999. He is currently a PhD student in Mechanical Engineering Department, University of Washington. His research interest is microelectromechanical systems using piezoelectric thin films.

Cheng-Chun Lee (Ryan) received a BSME degree from National Chiao-Tung University, Taiwan, in 1995, and an MS degree in Aeronautics and Astronautics Engineering from the University of Washington, Seattle, USA, in 2001. He is currently a PhD student in Mechanical Engineering Department, University of Washington. His interest of study is MEMS.

Guozhong Cao is an Associate Professor of Materials Science and Engineering and Mechanical Engineering, University of Washington. He received his PhD from Eindhoven University of Technology in 1991 and was appointed to UW faculty in 1996. His major awards include the college Outstanding Educator Award in 1999, and the University Distinguished Teaching Award in 2000. He has published over 150 refereed papers in a wide range of materials science field, edited three conference proceedings, and authored a book Nanostructures and Nanomaterials: Synthesis, Properties and Applications.

I.Y. Shen (Steve) is a Professor of Mechanical Engineering Department of the University of Washington. He received his PhD degree in Mechanical Engineering from the University of California, Berkeley. His general research area is vibration, sensing, and actuation. In particular, his expertise includes PZT thin-film micro-sensors/actuators and spindle/rotor dynamics. In the areas of PZT thin films, he is developing micro-sensors and actuators for future medical devices. In the area of spindle and rotor dynamics, he is developing computational algorithms to predict vibration of complex rotating machines, such as hard disk drives and turbine engines. For his 14-year academic career in US, Professor Shen has published more than 50 archival journal papers in his field and more than 50 conference papers.